Geophysical Research Letters

RESEARCH LETTER
10.1029/2018GL080695

Special Section:
Midlatitude Marine Heatwaves: Forcing and Impacts

Impact of Colored Dissolved Materials on the Annual Cycle of Sea Surface Temperature: Potential Implications for Extreme Ocean Temperatures

Anand Gnanadesikan[1], Grace E. Kim[1,2], and Marie-Aude S. Pradal[1]

[1]Morton K. Blaustein Department of Earth and Planetary Sciences, Johns Hopkins University, Baltimore, MD, USA, [2]NASA Goddard Spaceflight Center, Greenbelt, MD, USA

Abstract Because colored dissolved materials (CDMs) trap incoming sunlight closer to the surface, they have the potential to affect sea surface temperatures. We compare two models, one with and one without CDMs, and show that their presence leads to an increase in the amplitude of the seasonal cycle over coastal and northern subpolar regions, which may exceed 2 °C. The size and sign of the change are controlled by the interplay between enhanced shortwave heating of the surface, shading and cooling of the subsurface, and the extent to which these are connected by vertical mixing. The changes in the seasonal cycle largely explain changes in the range of temperature extremes, an aspect of climate with important implications for ecosystem cycling. The modeled changes associated with CDMs have an intriguing resemblance to the observed trend in the annual cycle seen in recent decades, suggesting that more attention be paid to the role of "ocean yellowing" in global change.

Plain Language Summary Colored detrital materials produced by decay of organic matter turn the oceans yellow and trap light closer to the surface. This results in more heating of the surface but less heating of the ocean interior during the summer months. As a result, colder water is mixed up to the surface in winter months, and the annual cycle of sea surface temperature increases. The pattern of this change resembles the observed trend in the annual cycle of SST, which is particularly important in coastal areas where it may result in driving marine heatwaves that drive changes in ecosystem structure. Our work suggests that more attention to ocean optics and mixed layer dynamics will be essential to properly understanding such changes in extreme temperatures.

Key Points:
- By changing the vertical distribution of solar heating colored dissolved materials change the annual cycle of sea surface temperatures
- Changes in the annual cycle of sea surface temperatures dominate changes in temperature extremes
- The spatial pattern of changes in the annual cycle driven by adding colored dissolved materials to a model resembles observed trends

Supporting Information:
- Supporting Information S1

Correspondence to:
A. Gnanadesikan,
gnanades@jhu.edu

Citation:
Gnanadesikan, A., Kim, G. E., & Pradal, M.-A. S. (2019). Impact of colored dissolved materials on the annual cycle of sea surface temperature: Potential implications for extreme ocean temperatures. *Geophysical Research Letters*, *46*, 861–869. https://doi.org/10.1029/2018GL080695

Received 29 SEP 2018
Accepted 10 JAN 2019
Accepted article online 15 JAN 2019
Published online 29 JAN 2019

1. Introduction

The presence of scatterers and absorbers in ocean water results in concentrating the absorption of sunlight closer to the surface than in pure water. Almost all Earth System Models operationally run for climate projection assume that this absorption depends only on the concentration of chlorophyll (Manizza et al., 2005; Morel & Antoine, 1994) This so-called bio-optical approximation breaks down in coastal regions, where colored dissolved materials (CDMs) and detrital materials dominate absorption (Kim et al., 2015; Siegel et al., 2005). Coastal waters have long been known to contain colored materials, often associated with the breakdown of organic material (Nelson et al., 1998, 2004). These materials tend to absorb most strongly at the shorter wavelengths associated with blue-green and ultraviolet light. One result of this absorption is to make the water look yellow (Jerlov, 1950). A more subtle effect arises from the fact that CDM absorbs in exactly the band where pure water is most transparent to light and so has a disproportionate impact on the trapping of solar heating (Kim et al., 2015).

In this paper, we examine the impact of this change in heating on sea surface temperatures (SSTs). We do this by parameterizing the impact of CDM in a coupled Earth System Model and then running two versions of this model, one with CDM and one without. Section 2 describes the model, and the term balances within it. Section 3 shows how the presence of CDM affects both the annual cycle of SSTs and the range of extreme SSTs expected during a 30-year climatology. Section 4 considers implications of this result, comparing the pattern of CDM-driven changes in SST range to those associated with global warming and, intriguingly, with observations.

2. Methods

2.1. Computational Model

Our baseline model is the GFDL ESM2Mc (Galbraith et al., 2011), a coarse-resolution version of the GFDL ESM2M model (Dunne et al., 2012) used in the Coupled Model Intercomparison Project version 5. ESM2Mc has an approximately 3° × 2° ocean coupled to an approximately 3° atmosphere, similar in resolution to state-of-the-art-coupled climate models in the second and third assessment reports. However, relative to these generations of models ESM2Mc has updated parameterizations of many features of ocean and atmospheric physics.

The physical model is coupled to the Biology-Light-Iron-Nutrient-Gasses model (Galbraith et al., 2010), which tracks macronutrient, micronutrient, and dissolved organic matter, carbon, and oxygen as prognostic tracers. The model uses the micronutrient, macronutrient, and modeled light level to compute a phytoplankton growth rate. Chlorophyll-to-carbon ratios are adjusted so that light uptake rates match nutrient uptake rates (Geider et al., 1997). The growth rate is then fed into a highly parameterized biology to compute a quasi-equilibrium biomass. The growth rate and biomass are then combined to produce uptake and recycling rates. A key aspect of this highly parameterized biology is an allometric (size-dependent) representation of grazing (Dunne et al., 2005), which enforces a relatively realistic shift from a low-export high-recycling ecosystem dominated by small phytoplankton in the subtropical gyre to a high-export-low-recycling ecosystem dominated by high biomass in highly productive waters.

The absorption of solar radiation in ESM2Mc is parameterized as follows. Half of the net downward flux of visible radiation is partitioned into a blue-green component I_{bg} and half into a yellow-red component, I_{yr}. Within the model each of these components is attenuated with a diffuse attenuation coefficient $I_{\{bg,\,yr\}}$ so that the shortwave heating rate Q_{SW} is

$$Q_{SW} = \frac{\partial}{\partial z}\left(I_{bg} + I_{yr}\right) = k_{bg} * I_{bg} + k_{yr} I_{yr} \tag{1}$$

(with z defined positive upward). In the original version of ESM2Mc we used the parameterization of Manizza et al. (2005):

$$k_{yr} = 0.225 + 0.037 * chl^{0.629}, \tag{2a}$$

$$\mathrm{k_{bg}} = 0.0232 + 0.074 * \mathrm{chl}^{0.674}, \tag{2b}$$

where *chl* is the chlorophyll concentration, which is predicted by the model. Kim et al. (2015) used the NASA bio-Optical Marine Dataset (Werdell & Bailey, 2005), which includes measurements of chl, CDM, and diffuse attenuation coefficient $k(\lambda)$ to fit a CDM-dependent parameterization for the blue-green component of sunlight:

$$k_{bg} = 0.0232 + 0.0513 * \mathrm{chl}^{0.668} + 0.71 * a_{dg}(443\ \mathrm{nm})^{1.13}, \tag{3}$$

where a_{dg} is the absorption coefficient associated with detrital and dissolved organic materials (i.e., CDM). The logarithm of a_{dg} estimated from the SeaWiFs satellite is shown in Figure 1a, showing that it is small in the middle of gyres (adding less than 0.01 m^{-1} to the diffusive attenuation coefficient of water for blue-green light) and large in coastal regions and the Arctic.

We performed two sets of experiments with our new parameterization. First, we took a version of ESM2Mc, which had been initialized with modern ocean hydrography and run out for 1,500 years using the old optical parametrization with greenhouse gasses (methane, carbon dioxide, and nitrous oxide) and aerosols (black carbon, sulfate aerosol, organic carbon, and eight size classes of dust) fixed at 1,860 values. At that point the optical parameterization was changed, and two cases were started. In our control model (denoted in the text as CDM + Chl), we set a_{dg} to the values shown in Figure 1a. In the second case, denoted as Chl-Only, we set a_{dg} to zero. Both simulations were then run out for 900 years. While there are some drifts in the deep ocean, surface temperatures come to equilibrium after about 100 years (Kim et al., 2018)—though in order to be cautious we look only at the last 700 years of the simulation. Differences between the CDM + Chl and Chl-only simulations thus show the total impact of adding CDM to the Earth System

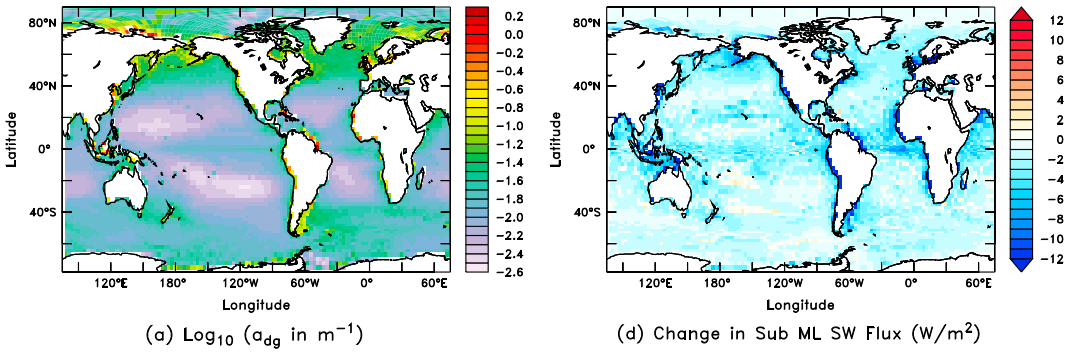

Figure 1. Distribution and radiative impact of colored dissolved material (CDM). (a) Log_{10} of absorption coefficient (in m^{-1}) associated with CDM at 443-nm wavelength (values with log $a_{dg} > -1.6$ indicate CDM absorption is more important than pure water at this wavelength). (b) Annual mean change in penetration of solar radiation below mixed layer in $\mathrm{W/m}^2$ CDM + Chl simulation—Chl-only simulation.

Model. The net impact on radiation penetrating below the depth of the boundary layer is shown in Figure 1b. Higher CDM absorption decreases the escape of light from the mixed layer by more than 10 $\mathrm{W/m}^2$ in coastal areas.

The models have a reasonable seasonal cycle over most of the global ocean. Figure S1a shows the annual amplitude of the annual cycle observed from the Reynolds OISST product, with peaks associated with the boundary current extension regions and low variability in the tropical Pacific. The models largely reproduce this pattern away from the Southern Ocean. In the Southern Ocean, a failure to properly simulate mid-to-low summertime clouds results in a warm bias during this season (Delworth et al., 2006), which largely disappears during the winter (our control model has a reasonable simulation of wintertime sea ice extent). The zonal-mean average of the annual temperature range shows good agreement north of about 20°S.

2.2. Budget Terms

In order to understand changes in the annual cycle, we also present detailed heat balances at various locations. Within any box in the water column, the heat balance associated with the temperature tendency can be written:

$$Q_{total} = \rho\, c_p \Delta z \left(\frac{\partial T}{\partial t}\right)_{total} = \left\{ \left(\frac{\partial T}{\partial t}\right)_{advect} + \left(\frac{\partial T}{\partial t}\right)_{neutral} + \left(\frac{\partial T}{\partial t}\right)_{submeso} + \left(\frac{\partial T}{\partial t}\right)_{vdiff} + \left(\frac{\partial T}{\partial t}\right)_{nonlocalKPP} + \left(\frac{\partial T}{\partial t}\right)_{SWpen} \right\} \rho\, c_p \Delta z. \tag{4}$$

The left-hand side refers to the total heating/cooling. The first term on the right-hand side is the tendency due to the advection of temperature within the model in all three dimensions by the resolved flow at the grid spacing. The $\left(\frac{\partial T}{\partial t}\right)_{neutral}$ term includes the temperature impacts from both the Gent and McWilliams (advective) and Redi diffusion (along-isopycnal mixing) terms (Griffies, 1998). The third term is submesocale mixing following Fox-Kemper et al. (2011), which parameterizes the overturning associated with submesoscale eddies whose source of energy is the horizontal density gradients within the mixed layer. The eddy terms can be combined as

$$Q_{eddy} = \rho\, c_p \Delta z \left(\frac{\partial T}{\partial t}\right)_{eddy} = \rho\, c_p \Delta z \left\{ \left(\frac{\partial T}{\partial t}\right)_{neutral} + \left(\frac{\partial T}{\partial t}\right)_{submeso} \right\}. \tag{5}$$

Vertical mixing (the fourth and fifth terms on the RHS of equation (4) as described in Large et al. (1994)) follows the basic pattern suggested by Troen and Mahrt (1986) for the atmospheric boundary layer, which represents the associated heat fluxes as

$$Q_{vmix} = \rho c_p \Delta z \left(\frac{\partial T}{\partial t}\right)_{Vmix} = \rho c_p \Delta z \frac{\partial}{\partial z} K_v \left(\frac{\partial T}{\partial z} - \gamma\right) = \rho c_p \left\{ \left(\frac{\partial T}{\partial t}\right)_{vdiff} + \left(\frac{\partial T}{\partial t}\right)_{nonlocalKPP} \right\}, \quad (6)$$

where K_v is a vertically varying mixing coefficient and $\gamma(z)$ parameterizes a "countergradient" term that allows for transport by large eddies that feel the large-scale gradient across the boundary layer rather than the local gradient (which may have the opposite sign). While these terms are saved out separately in the model, we combine them for our analysis. The final term in equation (4) is a source term from penetrating shortwave radiation, which removes heat deposited in the surface layer and redistributes it through the water column—as shown in equation (1).

3. Results

We might expect that the additional impact of CDM in trapping heat near the surface would lead to warmer summers. As seen in Figure 2a, the SST during the warmest month over the year does rise in regions such as the Pacific west coast, Baltic Sea, and NE Atlantic. However, noted in previous work (Kim et al., 2016, 2018), absorbing more heat near the surface means that less heat is absorbed at depth. As a result subsurface waters are cooler and, when exposed in the wintertime, drive a seasonal cooling (Figure 2c). When combined (Figure 2e), adding the absorption due to CDM results in an expanded annual range of SSTs throughout the subpolar oceans in both hemispheres and the subtropical Atlantic. In the polar Arctic, the wintertime cooling CDM leads to an expansion and thickening of sea ice (described in Kim et al., 2016), which decreases the annual range.

These changes in the seasonal cycle are reflected by changes in extreme temperatures. We define extreme temperatures as 96.7th percentile of monthly mean temperatures during the warmest month and the 3.3rd percentile of the coldest months taken over 700 years of model simulation. We choose the percentile threshold to correspond roughly to the warmest and coldest months we might expect to find in a standard 30-year climatology. The presence of CDM clearly results in an increase in extreme warm temperatures (Figure 2b) in coastal regions, with peak values reaching 1.5 °C. Similarly, the coldest months (Figure 2d) get colder. As a result the range of extreme temperatures (difference of high warm season and low cold season; Figure 2f) increases by up to 3.5 °C. As seen in Figure S2a in the supporting information the changes in annual range explain about 75% of the change in extreme range. The difference between the two (Figure S2b) reveals a complex spatial pattern of change, which does not neatly project onto a single mode of climate variability. Analysis of changes in the statistical distribution of SST with the seasonal cycle removed reveals a complex interplay between changes in variance, skew, and kurtosis (all of which have the potential to affect the extreme range) across different sites.

In order to understand why the annual cycle of temperature changes, we turn to the term balances that govern the changes in the seasonal cycle between our Chl + CDM and Chl-Only simulations as described in the methods. We consider four points (denoted by the blue numbers in Figure 3d) that illustrate different sorts of balances. The simplest balance is shown in Figure 3a, showing a point corresponding to the center of the Baltic Sea. At this location the addition of CDM produces an enhanced seasonal cycle, with more warming during the summer and more cooling during the winter. The CDM + Chl simulation has much less penetration of SW radiation than Chl-Only simulation (red line), heating the surface layer by up to 40 W/m^2. However, changes in mixing within the mixed layer (green line) tend to oppose this change in heating. The sum of the two (dark blue line) shows that shortwave heating wins during the summer but that during the winter the net impact of subsurface cooling is mixed back up to the surface. One-dimensional balances basically explain the entire change in seasonal cycle at this location, as the advective (light blue line) and lateral diffusive (magenta line) terms are relatively small.

One dimensional balances explain the bulk of annual change over much of the globe, but by no means everywhere (Figure S3). In the Kuroshio Extension (Figure 3b), vertical mixing has an annual cycle in the opposite sense as shortwave absorption but actually ends up positive during the winter, so that one dimensional processes actually result in additional heating. The annual cycle in heating and cooling (black line) still shows cooling during this time period and is strongly influenced by an annual cycle in advection (light blue line), with more cold water being advected into the region in the winter and more warm water in the summer.

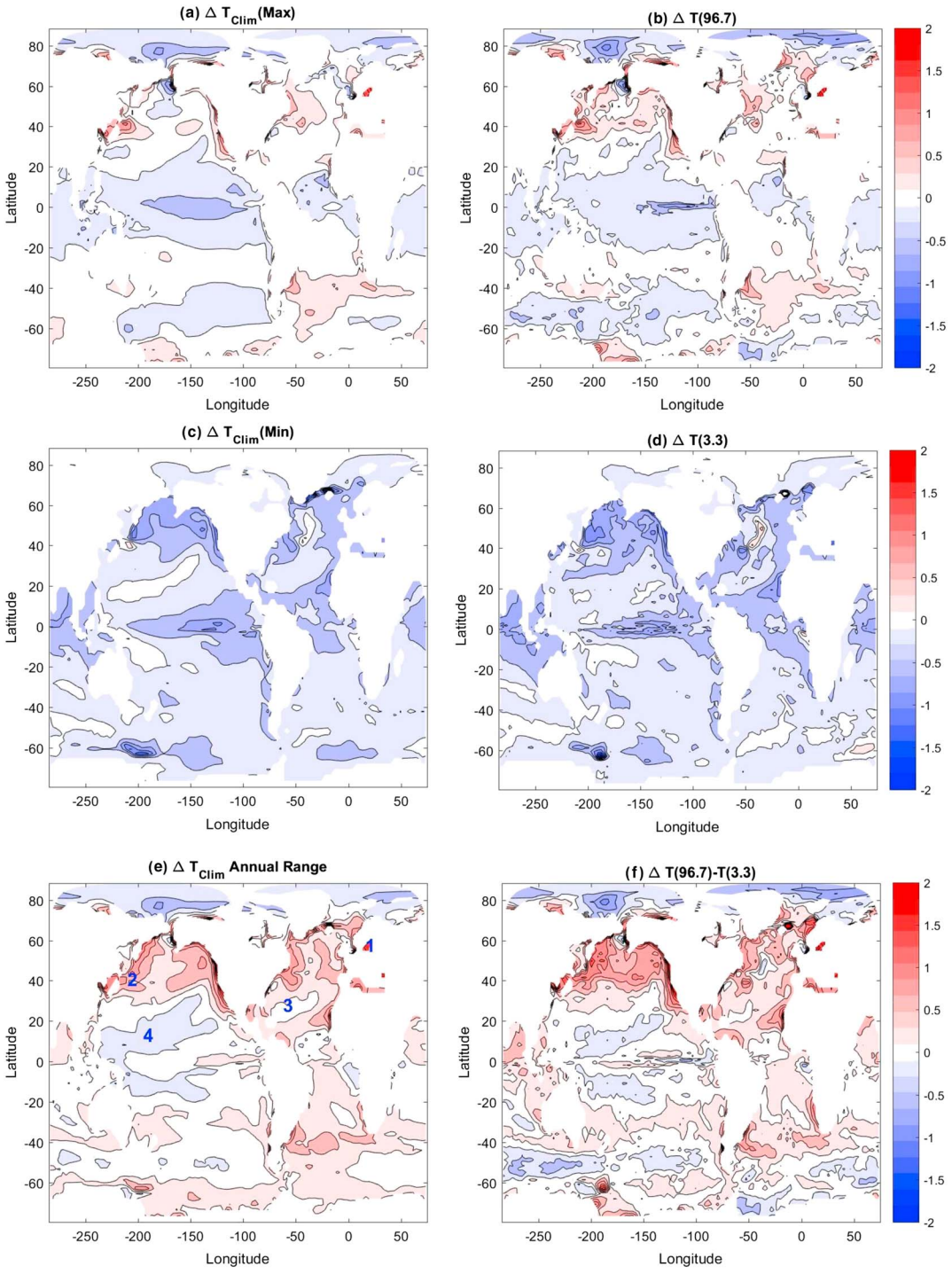

Figure 2. Changes in sea surface temperature associated with adding colored dissolved material to the model. (a) Change during the warmest climatological month. (b) Change of the 96.7 percentile of warmest month corresponding to warmest month during a 30-year climatology. (c) Change during the coldest climatological month. (d) Change of the 3.3 percentile of coldest month corresponding to coldest month during a 30-year climatology. (e) Change in annual sea surface temperature range (a minus c). (f) Change in range of extreme temperatures (b minus d).

In the subtropical Atlantic (Figure 3c) the vertical balance overpredicts the changes in heat flux associated with surface temperature change. At this site, the vertical balance is compensated by the lateral mixing term, which is dominated by submesoscale restratification of the mixed layer. Submesoscale restratification goes as the square of the mixed layer depth, which at this location reaches 200 m during the wintertime,

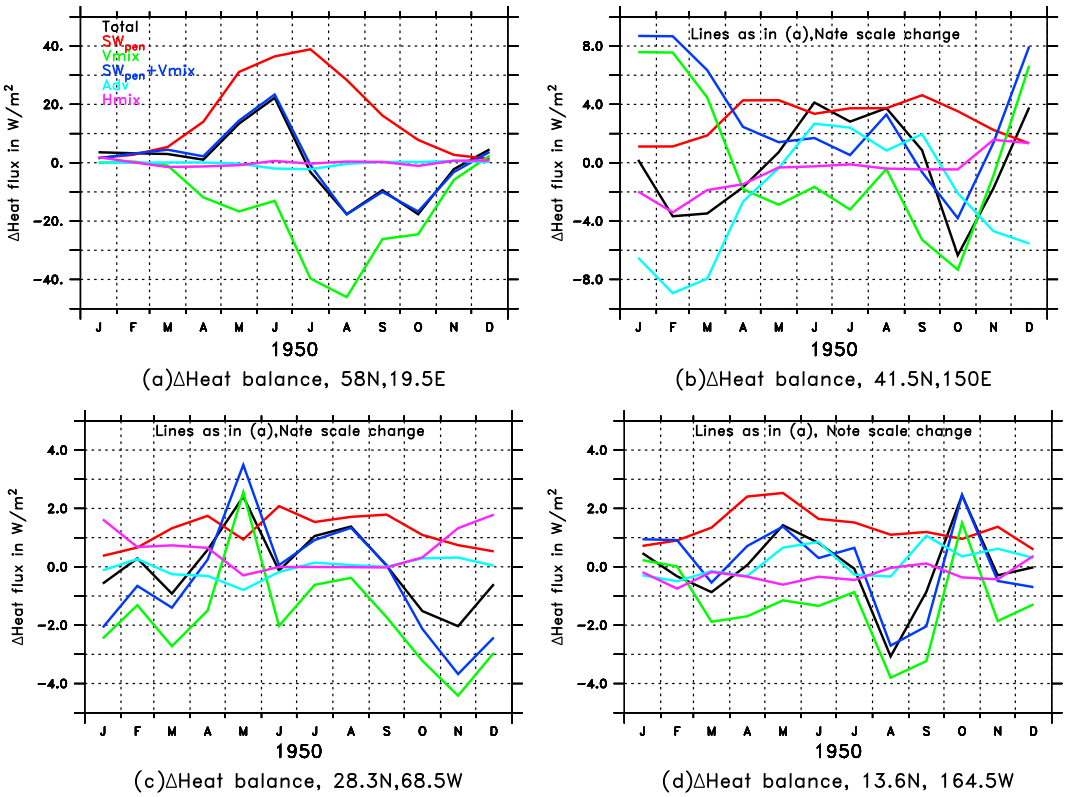

Figure 3. Changes in the heat balance of the topmost model layer associated with adding colored dissolved material, as given in equations (1) and (4). Line colors denote total heating Q_{total} (black), additional trapping of shortwave radiation Q_{SW} (red lines), vertical mixing Q_{Vdiff} (green lines), the sum of $Q_{SW} + Q_{Vdiff}$ representing all 1-D mixed layer processes (dark blue lines), three-dimensional advection (light blue), and lateral mixing associated with either mesoscale diffusion and submesoscale diffusion Q_{eddy} (purple). Sites are (a) 58°N, 19.5°E, central Baltic Sea. (b) 41°N, 150°E, Kuroshio extension, illustrating a regime where advection is important. (c) 28.3°N, 65°W, central subtropical Atlantic, illustrating a regime where submesoscale restratification is important. (d) 13.6°N, 164.5°W tropical Pacific, illustrating a regime where the annual cycle decreases.

deeper than other sites considered in Figure 3. Finally, at 13°N, 160°W (Figure 3d) the change in the annual cycle in vertical mixing is larger than the change in penetrating shortwave radiation, resulting in a reduced annual cycle in the presence of CDM.

4. Discussion

The fact that CDM has the ability to change both annual and extreme temperature ranges has wide implications beyond physical oceanography. As many organisms exist within a preferred temperature range, prolonged conditions outside of this range can result in significant mortality (Pearson & Dawson, 2003). Extremes of high temperatures have been associated with ecosystem shifts across the globe, from the tropics, where marine heat waves have driven coral bleaching (Strong et al., 2006), to the Mediterranean where a 2003 heat wave was associated with mass mortality of benthic invertabrates (Garrabou et al., 2009). On the other hand, extremely cold winters have been shown to kill larval fish such as the Atlantic Croaker (Lankford & Targett, 2001). The dynamics behind such changes in temperature extremes are still not well understood (Frölicher & Laufkötter, 2018).

Changes in annual cycling may play a role in such extreme events. Looking at the Reynolds optimally interpolated SST product (Reynolds et al., 2007), we see that both the annual range of SST (defined as the maximum monthly average minus the minimum monthly average; Figure 4a) and the range associated with the annual harmonic of SST (computed by fitting a sinusoid with period of 1 year to the SST at each point, taking the peak to trough range of the result for each year, and then looking for trends in the amplitude; Figure 4b) show changes over the past 36 years. Outside of the Arctic, both of these patterns have a significant similarities with the changes associated with CDM, with both patterns showing increases in the annual

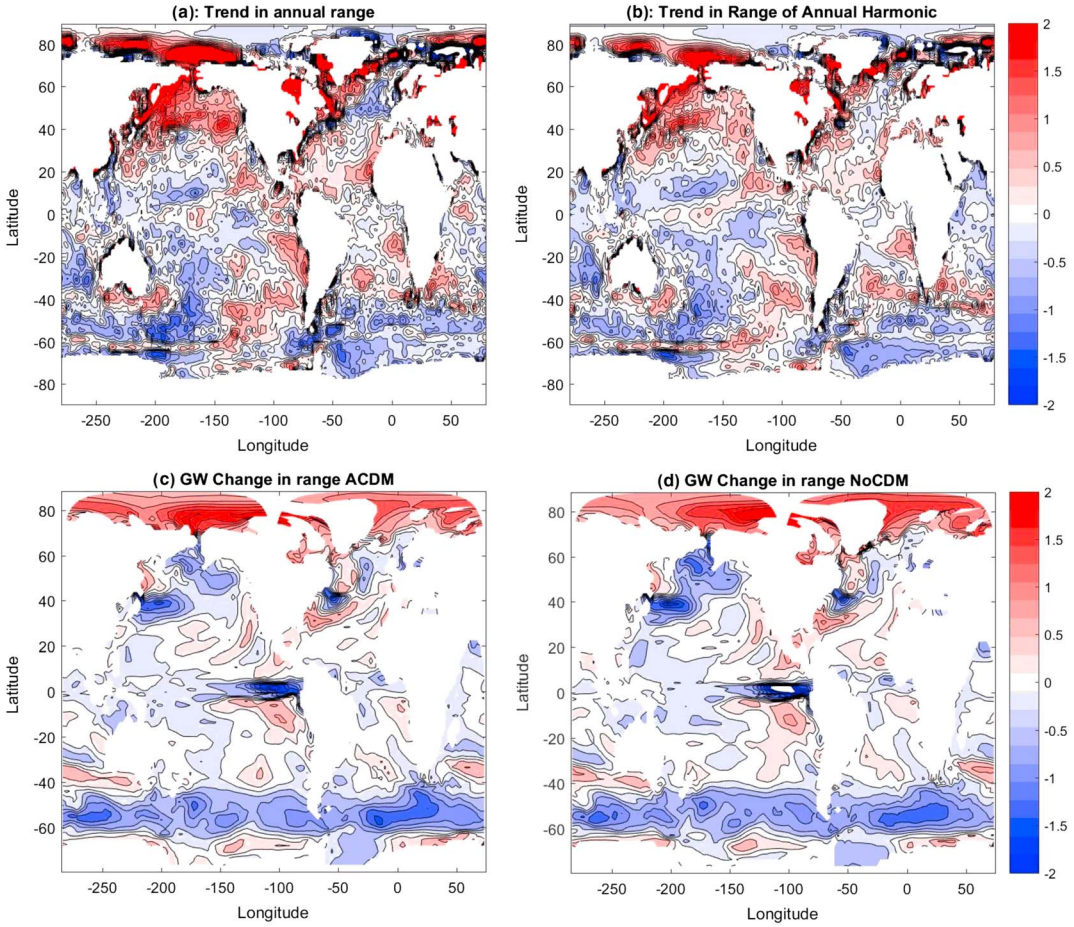

Figure 4. Changes in the annual sea surface temperature range. (a) Observed using the Reynolds OISST product (Reynolds et al., 2007) from 1982–2017 (trend in annual maximum-annual minimum). (b) Trend associated with the annual harmonic of the Reynolds sea surface temperature from 1982–2017. (c) Associated with doubling CO_2 (GW) in the presence of colored dissolved material (ACDM). (d) Associated with doubling CO_2 (GW) in the absence of colored dissolved material (NoCDM).

cycle in the North Pacific subpolar gyre, the coastal regions of the North Atlantic, including the Baltic and Mediterranean Seas and the coastal upwelling zones such as the Peru and Benguela currents and decreases in the Pacific subtropics.

We do not mean to suggest that the agreement between Figures 4a and 4b and 2e and 2f means that recent observed increases in the seasonal cycle are necessarily driven by an increase in CDM. First, the observed changes appear to be larger than what our model predicts with CDM alone. Moreover, while the observational record is currently too short and too uncertain to establish whether CDM is increasing or decreasing in the ocean as a whole over multidecadal time scales, it is certainly *not* the case that there was no CDM in the ocean before 1982.

However, it is also worth noting that our model has a relatively coarse resolution in the vertical (eight boxes cover the top 100 m). Under weak winds the diurnal summertime mixed layer can be very shallow and have temperature excursions of 2–3 °C. Representing such mixed layers in climate models can require very high resolution (as fine as 1 m) in the vertical (Bernie et al., 2006; Sui et al., 1997). In such regions, the impact of changes in shortwave absorption will be even larger than seen here and our model will likely underestimate the impact of such changes on climate. Moreover, there is evidence of increasing concentration of dissolved organic carbon in inland waters (lakes and streams) and that in some regions a larger fraction of this dissolved organic carbon is becoming more tinted (Pagano et al., 2014; Strock et al., 2017; Worrall & Burt, 2010). A few regions, most notably the Gulf of Maine, have seen both documented increase in CDM and an increase in temperature ranges (Balch et al., 2016; Thomas et al., 2017).

It is also interesting that the patterns of change in SST annual range are quite *different* than those seen from global warming alone. Figures 4c and 4d show the changes in SST annual range from the first 5 years of a three-member ensemble immediately after atmospheric carbon dioxide is doubled. The annual range changes with and without CDM are very similar (with a correlation coefficient of 0.95 and regression coefficient of 1.015) and are poorly correlated with the pattern of annual change associated with CDM (the correlation coefficient between the fields shown in Figures 4c and 4d and that in 2e is −0.19). This suggest that it is important how heat is added to the surface ocean—changing the trapping of outgoing longwave radiation via increasing greenhouse gasses has a different signature than increasing the trapping of shortwave radiation in the mixed layer.

Our results have a number of important implications for observing and modeling the Earth. The first is that they highlight the importance of changes in the amplitude of the annual cycle. In many locations, these changes are significantly larger than annual mean changes. As such changes in temperature can have important implications for phenology, adequately predicting changes in marine ecosystem structure requires more attention needs to be paid to the mechanisms driving the amplitude of the annual cycle. Our second point is that the processes that establish the profile of solar heating and its redistribution in the vertical are key to understanding these seasonal changes. Recent changes in annual range are broadly consistent with a mechanism in which more heat is trapped at the surface during the summer and less is brought up during the winter—and thus, changes in ocean color could potentially play a role.

Advancing such understanding will require more comprehensive long-term monitoring of CDM. Currently, it is difficult to detect trends in ocean color properties as there are relatively few in situ time series stations, and satellite-based observations must be corrected for poorly known impacts of atmospheric absorption (Blondeau-Patissier et al., 2014). Such problems are particularly challenging in coastal environments where the spectral properties of CDM as well as its concentrations may vary with time. Modeling such changes may require much higher vertical resolution than is standard in modern climate models, suggesting a further area for investigation. It will also require understanding changes in nutrient deposition (Doney, 2010), which would be expected to enhance the production of CDM as well as changes in the degradation of this key absorber.

Acknowledgments
This work was supported by NOAA under Grant NA15OAR4310172 and NSF under Grant EAR- 1135382 (A. G. and M. A. P.) by NASA under the NASA Earth and Space Science Fellowship Program Grant NNX14AK98H (G. K.). We thank Tim DeVries and an anonymous reviewer for useful comments. Data used to create the figures in these papers are available via the Johns Hopkins University dataverse at doi:10.7281/T1/DG7RDP.

References

Balch, W., Huntington, T., Aiken, G., Drapeau, D., Bowler, B., Lubelczyk, L., & Butler, K. (2016). Toward a quantitative and empirical dissolved organic carbon budget for the Gulf of Maine, a semienclosed shelf sea. *Global Biogeochemical Cycles*, *30*, 268–292. https://doi.org/10.1002/2015GB005332

Bernie, D. J., Woolnough, S. J., Slingo, J. M., & Guilyardi, E. (2006). Modeling diurnal and intraseasonal variability of the ocean mixed layer. *Journal of Climate*, *18*(8), 1190–1202.

Blondeau-Patissier, D., Gower, J. F., Dekker, A. G., Phinn, S. R., & Brando, V. E. (2014). A review of ocean color remote sensing methods and statistical techniques for the detection, mapping and analysis of phytoplankton blooms in coastal and open oceans. *Progress in Oceanography*, *123*, 123–144. https://doi.org/10.1016/j.pocean.2013.12.008

Delworth, T. L., Broccoli, A. J., Rosati, A., Stouffer, R. J., Balaji, V., Beesley, J. A., et al. (2006). GFDL's CM2 global coupled climate models. Part I: Formulation and simulation characteristics. *Journal of Climate*, *19*(5), 643–674. https://doi.org/10.1175/JCLI3629.1

Doney, S. C. (2010). The growing human footprint on coastal and open-ocean biogeochemistry. *Science*, *328*(5985), 1512–1516. https://doi.org/10.1126/science.1185198

Dunne, J. P., Armstrong, R. A., Gnanadesikan, A., & Sarmiento, J. L. (2005). Empirical and mechanistic models of particle export. *Global Biogeochemical Cycles*, *19*, GB4026. https://doi.org/10.1029/2004GB002390

Dunne, J. P., John, J. G., Adcroft, A. J., Griffies, S. M., Hallberg, R. W., Shevliakova, E., et al. (2012). GFDL's ESM 2 global coupled climate-carbon earth system models. Part I: Physical formulation and baseline simulation characteristics. *Journal of Climate*, *25*(19), 6646–6665. https://doi.org/10.1175/JCLI-D-11-00560.1

Fox-Kemper, B., Danabasoglu, G., Ferrari, R., Griffies, S. M., Hallberg, R. W., Holland, M. M., et al. (2011). Parameterization of mixed layer eddies. III: Implementation and impact in global ocean climate simulations. *Ocean Modelling*, *39*(1–2), 61–78. https://doi.org/10.1016/j.ocemod.2010.09.002

Frölicher, T. L., & Laufkötter, C. (2018). Emerging risks from marine heat waves. *Nature Communications*, *9*(1), 650. https://doi.org/10.1038/s41467-018-03163-6

Galbraith, E. D., Gnanadesikan, A., Dunne, J. P., & Hiscock, M. R. (2010). Regional impacts of iron-light colimitation in a biogeochemical model. *Biogeosciences*, *7*(3), 1043–1064. https://doi.org/10.5194/bg-7-1043-2010

Galbraith, E. D., Kwon, E. Y., Gnanadesikan, A., Rodgers, K. R., Griffies, S. M., Bianchi, D., et al. (2011). The impact of climate variability on the distribution of radiocarbon in CM2Mc—A new earth system model. *Journal of Climate*, *24*(16), 4230–4254. https://doi.org/10.1175/2011JCLI3919.1

Garrabou, J., Coma, R., Bensoussan, N., Bally, M., Chevaldonné, P., Cigliano, M., et al. (2009). Mass mortality in northwestern Mediterranean rocky benthic communities: Effects of the 2003 heat wave. *Global Change Biology*, *15*(5), 1090–1103. https://doi.org/10.1111/j.1365-2486.2008.01823.x

Geider, R. J., MacIntyre, H. L., & Kana, T. M. (1997). Dynamic model of phytoplankton growth and acclimation: Responses of the balanced growth rate and the chlorophyll a: Carbon ratio to light, nutrient-limitation and temperature. *Marine Ecology Progress Series*, *148*, 187–200. https://doi.org/10.3354/meps148187

Griffies, S. M. (1998). The gent–McWilliams skew flux. *Journal of Physical Oceanography*, *28*(5), 831–841. https://doi.org/10.1175/1520-0485(1998)028<0831:TGMSF>2.0.CO;2

Jerlov, N. G. (1950). Ultraviolet radiation in the ocean. *Nature*, *166*(4211), 111–112. https://doi.org/10.1038/166111a0

Kim, G. E., Gnanadesikan, A., del Castillo, C. E., & Pradal, M. A. (2018). Upper ocean cooling in a coupled climate model due to light attenuation by yellowing materials. *Geophysical Research Letters*, *45*, 6134–6140. https://doi.org/10.1029/2018GL077297

Kim, G. E., Gnanadesikan, A., & Pradal, M. A. (2015). Quantifying the biological impact of surface ocean light attenuation by colored detrital matter in an ESM using a new optical parameterization. *Biogeosciences*, *12*(16), 5119–5132. https://doi.org/10.5194/bg-12-5119-2015

Kim, G. E., Gnanadesikan, A., & Pradal, M. A. (2016). Increased surface ocean heating by colored detrital matter (CDM) linked to greater Northern Hemisphere ice formation in the GFDL CM2Mc ESM. *Journal of Climate*, *29*(24), 9063–9076. https://doi.org/10.1175/JCLI-D-16-0053.1

Lankford, T. E., & Targett, T. E. (2001). Low-temperature tolerance of age-0 Atlantic croakers: Recruitment implications for U.S. Mid-Atlantic estuaries. *Transactions of the American Fisheries Society*, *130*(2), 236–249. https://doi.org/10.1577/1548-8659(2001)130<0236:LTTOAA>2.0.CO;2

Large, W. G., McWilliams, J. C., & Doney, S. C. (1994). Oceanic vertical mixing: A review and a model with a nonlocal boundary layer parameterization. *Reviews of Geophysics*, *32*(4), 363–403. https://doi.org/10.1029/94RG01872

Manizza, M., Le Quéré, C., Watson, A. J., & Buitenhuis, E. T. (2005). Bio-optical feedbacks among phytoplankton, upper ocean physics and sea-ice in a global model. *Geophysical Research Letters*, *32*, L05603. https://doi.org/10.1029/2004GL020778

Maritorena, S., Siegel, D. A., & Peterson, A. R. (2002). Optimization of a semianalytical ocean color model for global-scale applications. *Applied Optics*, *41*(15), 2705–2714. https://doi.org/10.1364/AO.41.002705

Morel, A., & Antoine, D. (1994). Heating rate within the upper ocean in relation to its bio–optical state. *Journal of Physical Oceanography*, *24*(7), 1652–1665. https://doi.org/10.1175/1520-0485(1994)024<1652:HRWTUO>2.0.CO;2

Nelson, N. B., Carlson, C. A., & Steinberg, D. K. (2004). Production of chromophoric dissolved organic matter by Sargasso Sea microbes. *Marine Chemistry*, *89*(1–4), 273–287. https://doi.org/10.1016/j.marchem.2004.02.017

Nelson, N. B., Siegel, D. A., & Michaels, A. F. (1998). Seasonal dynamics of colored dissolved material in the Sargasso Sea. *Deep Sea Research Part I: Oceanographic Research Papers*, *45*(6), 931–957.

Pagano, T., Bida, M., & Kenny, J. E. (2014). Trends in levels of allochthonous dissolved organic carbon in natural water: A review of potential mechanisms under a changing climate. *Water*, *6*(10), 2862–2897. https://doi.org/10.3390/w6102862

Pearson, R. G., & Dawson, T. P. (2003). Predicting the impacts of climate change on the distribution of species: Are bioclimate envelope models useful? *Global Ecology and Biogeography*, *12*(5), 361–371. https://doi.org/10.1046/j.1466-822X.2003.00042.x.

Reynolds, R. W., Smith, T. M., Liu, C., Chelton, D. B., Casey, K. S., & Schlax, M. G. (2007). Daily high-resolution-blended analyses for sea surface temperature. *Journal of Climate*, *27*(21), 8221–8228. https://doi.org/10.1175/JCLI-D-14-00293.1

Siegel, D. A., Maritorena, S., Nelson, N. B., & Behrenfeld, M. J. (2005). Independence and interdependencies among global ocean color properties: Reassessing the bio-optical assumption. *Journal of Geophysical Research*, *110*, C07011. https://doi.org/10.1029/2004JC002527

Strock, K. E., Theodore, N., Gawley, W. G., Ellsworth, A. C., & Saros, J. E. (2017). Increasing dissolved organic carbon concentrations in northern boreal lakes: Implications for lake water transparency and thermal structure. *Journal of Geophysical Research: Biogeosciences*, *122*, 1022–1035. https://doi.org/10.1002/2017JG003767

Strong, A. E., Arzayus, F., Skirving, W., & Heron, S. F. (2006). Identifying coral bleaching remotely via coral reef watch—Improved integration and implications for changing climate, in coral reefs and climate change: Science and management. *Coastal and Estuarine Studies*, *61*, 18–26.

Sui, C., Li, X., Lau, K., & Adamec, D. (1997). Multiscale air-sea interactions during TOGA COARE. *Monthly Weather Review*, *125*(4), 448–462. https://doi.org/10.1175/1520-0493(1997)125<0448:MASIDT>2.0.CO;2

Thomas, A. C., Pershing, A. J., Friedland, K. D., Nye, J. A., Mills, K. E., Alexander, M. A., Record, N. R., et al. (2017). Seasonal trends and phenology shifts in sea surface temperature on the North American northeastern continental shelf. *Elementa: Science of the Anthropocene*, *5*(0), 48. http://doi.org/10.1525/elementa.240. https://doi.org/10.1525/elementa.240

Troen, I. B., & Mahrt, L. (1986). A simple model of the atmospheric boundary layer; sensitivity to surface evaporation. *Boundary-Layer Meteorology*, *37*(1–2), 129–148. https://doi.org/10.1007/BF00122760

Werdell, P. J., & Bailey, S. W. (2005). An improved in-situ bio-optical data set for ocean color algorithm development and satellite data product validation. *Remote Sensing of Environment*, *98*(1), 122–140. https://doi.org/10.1016/j.rse.2005.07.001

Worrall, F., & Burt, T. P. (2010). Has the composition of fluvial DOC changed? Spatiotemporal patterns in the DOC-color relationship. *Global Biogeochemical Cycles*, *24*, GB1010. https://doi.org/10.1029/2008GB003445